

MS No. S-2017-214.R1

# Service-Load Behavior of Precast/Prestressed Concrete Beams with Recycled Concrete Aggregates

by Michael R. Brandes and Yahya C. Kurama

*This paper describes an experimental investigation on the use of recycled concrete aggregates (RCAs) as replacement for coarse natural aggregates (NAs) in precast/prestressed concrete structures. Specifically, sustained service load tests were conducted on 18 pretensioned beams with two different levels of RCA (50% and 100% by aggregate volume), two sources of high-quality RCA (from both rejected precast members and a construction demolition recycling YARD), two different concrete mixture designs, concrete ages of 7 days and 28 days at superimposed service loading, and two different levels of prestressing (to result in beams that are uncracked or cracked under the superimposed load). The loss of prestress over time and midspan deflections of the beam specimens were monitored. Creep and shrinkage strains of accompanying concrete cylinders were also measured. The results showed that the effect of RCA on the service-load behavior of the beams was modest, even at full (100%) aggregate replacement. Additionally, the ability of current code approaches to estimate the measured immediate and sustained load deflections of the beams was not affected by the use of RCA.*

**Keywords:** creep; precast concrete; prestress loss; prestressed concrete; shrinkage; recycled concrete aggregate (RCA); sustained service load; time-dependent deflection.

## INTRODUCTION

While the use of recycled concrete aggregates (RCAs) is widespread as a sustainable alternative to coarse natural aggregates (NAs) in nonstructural concrete applications (for example, sidewalks and pavements), the effects of RCA in structural reinforced concrete members and assemblies (for example, beams, columns, and frames) are not as well known. The basic mechanical and time-dependent behavior of RCA concrete (that is, concrete made using RCA) is affected by the variability in the RCA material properties from different sources. Previous research has shown that this variability can be accounted for by using the RCA water absorption and deleterious material content such as wood and asphalt as predictors of the compressive strength, stiffness, creep, and shrinkage of RCA concrete.<sup>1,2</sup> RCA has a more significant impact on the concrete deformations than on the compressive strength. Therefore, the understanding of the long-term (sustained) service-load deflection behavior of RCA concrete structures remains one of the primary obstacles against increased use in structural applications. This paper focuses on this topic, specifically for precast/prestressed concrete structures.

Service-load tests of 18 simply supported pretensioned beams are presented, investigating the effects of varying amounts of RCA up to the full volume replacement of the coarse aggregate. Other experimental parameters include

the RCA source, superimposed service loading age, and prestress level. Two different sources of high-quality RCA from traditional construction demolition recycling waste and rejected precast concrete members are used. An important benefit of using rejected precast members is that precast concrete plants can use their own discarded products, thus achieving a more consistent RCA source (as compared with material from construction demolition recycling yards), while also reducing material transportation costs and space needed for the storage of concrete debris. Additionally, the effect of RCA on precast concrete can be closely monitored and controlled due to the quality-controlled and repetitive construction environment of the industry.

## RESEARCH SIGNIFICANCE

Previous research on the material properties of RCA concrete has shown that increased aggregate replacement leads to considerable decreases in the concrete stiffness as well as increases in the concrete creep and shrinkage strains.<sup>1-6</sup> Researchers have investigated the resulting increases in the immediate and long-term service-load deflections of non-prestressed RCA concrete beams.<sup>7-9</sup> However, to the best of the authors' knowledge, there has been no research on prestressed concrete structures with RCA. Because prestressing introduces compression into the concrete, demands on the material can be generally greater. For example, the increased compressive stresses can induce greater creep deformations in prestressed concrete. The use of discarded/rejected precast concrete<sup>10,11</sup> represents a significant opportunity as a source for clean RCA with consistent properties and high quality. This paper presents recent research that supports and contributes toward this vision.

## EXPERIMENTAL PROGRAM

The 18 beams in the experimental program were  $l = 19$  ft (5.79 m) long,  $b = 6$  in. (152 mm) wide, and  $h = 9$  in. (229 mm) deep (Fig. 1). The primary reinforcement consisted of two 0.5 in. (12.7 mm) diameter steel prestressing strands placed at a depth of  $d_p = 7.5$  in. (191 mm) from the top. Each beam was also reinforced with two U.S. Grade 60 No. 3 (Metric Grade 420 No. M10) longitudinal bars at the top, in addition to U.S. Grade 60 No. 3 (Metric Grade 420 No. M10)

*ACI Structural Journal*, V. 115, No. 3, May 2018.

MS No. S-2017-217.R1, doi: 10.14359/51702133, was received June 27, 2017, and reviewed under Institute publication policies. Copyright © 2018, American Concrete Institute. All rights reserved, including the making of copies unless permission is obtained from the copyright proprietors. Pertinent discussion including author's closure, if any, will be published ten months from this journal's date if the discussion is received within four months of the paper's print publication.

**Table 1—Aggregate properties**

Aggregate ID	Aggregate type	Specific gravity		Water absorption, % weight	Deleterious material, % weight	Target gradation
		Bulk dry	Saturated surface-dry			
FA2	Sand	—	2.62	0.90	—	MDOT No. 2NS
FA3	Limestone sand	—	2.80	0.60	—	MDOT No. 2NS
NA-CL2	Crushed limestone	2.61	2.68	0.60	—	MDOT No. 17A*
RCA-PC3	Rejected precast	2.44	2.52	3.39	<1	MDOT No. 17A*
RCA-T	Demolition waste	2.49	2.60	4.36	<1	MDOT No. 17A*

\*Exact target gradation was not met for these aggregates (refer to Fig. 2).

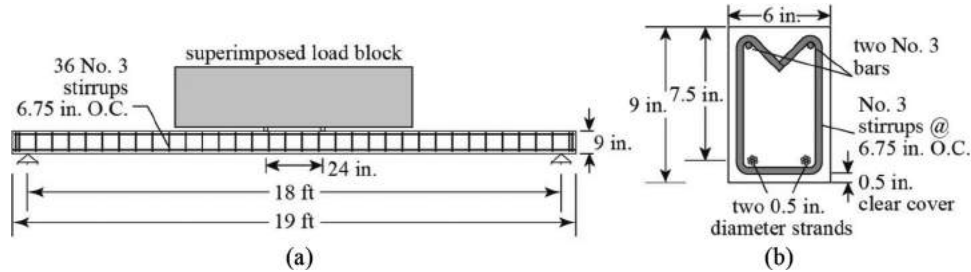


Fig. 1—Beam specimens: (a) elevation; and (b) cross section. (Note: 1 in. = 25.4 mm; 1 ft = 0.30 m.)

stirrups at 6.75 in. (171 mm) on center. The strands in 12 of the specimens were pre-tensioned (jacked) to a stress of  $f_{pj} = 0.7f_{pu}$  (where  $f_{pu} = 270$  ksi [1862 MPa] is the specified ultimate strand strength) to prevent immediate cracking of the bottom surface under the superimposed service load (consistent with Class U member definition in ACI 318<sup>12</sup>). The other six specimens were pre-tensioned to  $f_{pj} = 0.5f_{pu}$  to result in bottom concrete tensile stresses within the range defined for ACI 318 Class C (cracked) members under the superimposed service load. All 18 beams were designed to develop cracking on the top surface upon prestress transfer and were, therefore, reinforced with the two U.S. No. 3 (No. M10) top bars to control this cracking, as allowed by ACI 318.<sup>12</sup>

Table 1 shows the fine and coarse aggregates used in the research. Two different MDOT<sup>13</sup> No. 2NS sand types were used as fine aggregate (FA): a typical concrete sand (FA2) and limestone sand (FA3). The coarse natural aggregate (NA) was crushed limestone (NA-CL2). Two different RCA sources were used. The first source (RCA-PC3) was rejected hollow-core members at Kerkstra Precast, Inc., in Grandville, MI. The second source (RCA-T) was material from a traditional construction demolition waste recycling yard. The target gradation for all the coarse aggregates was MDOT<sup>13</sup> No. 17A; however, this target was not exactly achieved, as can be seen in Fig. 2. ASTM C127<sup>14</sup> and ASTM C128<sup>15</sup> were used to determine the specific gravity and water absorption for the coarse and fine aggregates, respectively. Both RCA sources were clean, with less than 1% deleterious materials. The choice of using high-quality RCA in the project was deliberate, as this would be the likely approach for the implementation of RCA in precast concrete (because of the rigorous quality requirements used in the industry).

The RCA concrete mixtures used in the beams were designed based on two target NA concrete mixtures. The dry weight proportions of these NA concrete mixtures are shown in Table 2. Mixture M-NA4 used typical Type I

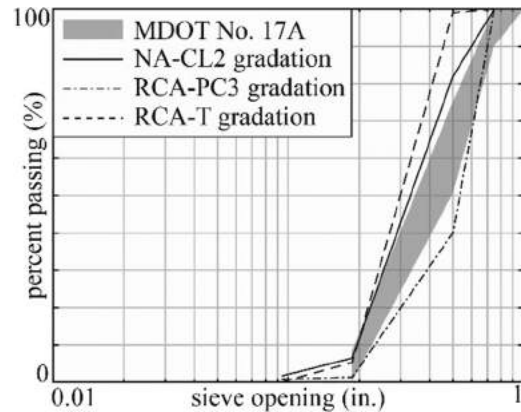


Fig. 2—Coarse aggregate gradation. (Note: 1 in. = 25.4 mm.)

portland cement and sand with a water-cement ratio ( $w/c$ ) of 0.34, while mixture M-NA5 used an alternative white Type I cement (typical of an “architectural” mixture) and limestone sand with  $w/c$  of 0.38. The concrete admixtures included a high-range water reducer (HRWR) and an air-entraining agent (AEA), which satisfied ASTM C494<sup>16</sup> (Types A and F) and ASTM C260,<sup>17</sup> respectively. The cement was ASTM C150<sup>18</sup> Type I portland cement; however, it was able to achieve high early-age strength gain (necessary in the precast industry) with a target spread of  $22 \pm 2$  in. ( $559 \pm 51$  mm) by using relatively low  $w/c$  and finely tuned proportions of admixtures (not listed in Table 2).

The RCA concrete mixtures were determined using the direct volume replacement (DVR) method<sup>1</sup> by replacing a selected volume of coarse NA with an equal volume of RCA according to

$$R = 1 - V_{NA}^{DVR} / V_{NA}^{NAC} \quad (1)$$

where  $R$  is volumetric replacement ratio;  $V_{NA}^{DVR}$  is volume of coarse natural aggregate in RCA concrete mixture; and

**Table 2—Dry-weight proportions for target NA concrete mixture designs (excluding admixtures)**

NA mixture ID	Water, <sup>*</sup> lb/yd <sup>3</sup>	Cement, lb/yd <sup>3</sup>	Cement type <sup>†</sup>	w/c	Coarse NA, <sup>‡</sup> lb/yd <sup>3</sup>	Coarse NA type <sup>‡</sup>	FA, <sup>§</sup> lb/yd <sup>3</sup>	FA type <sup>§</sup>
M-NA4	235	700.0	I-2	0.34	1600.0	NA-CL2	1420.0	FA2
M-NA5	262	700.0	I-3	0.38	1600.0	NA-CL2	1443.0	FA3

\*Required mixture water over saturated-surface-dry (SSD) condition of coarse and fine aggregates.

†Two different types of Type I cement were used.

‡Saturated-surface-dry (SSD) weights for coarse natural aggregates (NA).

§Saturated-surface-dry (SSD) weights for fine aggregates (FA).

Note: 1 lb/yd<sup>3</sup> = 0.59 kg/m<sup>3</sup>.

**Table 3—Dry-weight proportions for RCA concrete mixture designs**

RCA mixture ID	Target NA mixture ID <sup>*</sup>	RCA type	R, <sup>†</sup> %	w/c	Coarse NA, <sup>‡</sup> lb/yd <sup>3</sup>	Coarse RCA, <sup>‡</sup> lb/yd <sup>3</sup>
M-RCA15	M-NA4	RCA-PC3	50	0.34	800.0	752.2
M-RCA16	M-NA4	RCA-PC3	100	0.34	—	1504.5
M-RCA17	M-NA5	RCA-PC3	50	0.38	800.0	752.2
M-RCA18	M-NA5	RCA-PC3	100	0.38	—	1504.5
M-RCA19	M-NA4	RCA-T	50	0.34	800.0	776.1
M-RCA20	M-NA4	RCA-T	100	0.34	—	1552.2

\*Refer to Table 2.

†R is coarse aggregate replacement ratio (Eq. (1)).

‡Saturated-surface-dry (SSD) weights for NA and RCA.

Note: 1 lb/yd<sup>3</sup> = 0.59 kg/m<sup>3</sup>.

$V_{NA}^{NAC}$  is volume of coarse natural aggregate in NA concrete mixture. The DVR method ensures that for a given volume of concrete, the volumetric proportion of each component of the mixture remains constant between different RCA and NA concrete mixture designs. As described in Knaack and Kurama,<sup>1</sup> a similar level of workability (slump or spread) for RCA concrete and NA concrete can be achieved through this method as long as the difference between the water absorptions of RCA and NA is considered, as would be typical practice for concrete batching.

Two RCA concrete mixtures were determined by replacing the coarse aggregates in each NA concrete mixture at  $R = 0.5$  (that is, 50% volumetric replacement) and 1.0 (100% replacement). The dry-weight proportions for these mixtures are given in Table 3. The NA concrete mixtures (that is,  $R = 0$  mixtures in Table 2) serve as benchmark, while the  $R = 1.0$  mixtures represent the effect of full aggregate replacement and the  $R = 0.5$  mixtures represent intermediate replacement.

### Beam pretensioning and casting procedure

The 18 test specimens were cast in three series of six beams, listed in Table 4, at Kerkstra Precast, Inc. In the specimen nomenclature, the first letter “U” indicates uncracked (Class U) beams with  $f_{pj} = 0.7f_{pu}$ , while “C” indicates cracked (Class C) beams with  $f_{pj} = 0.5f_{pu}$ . The second letter of the nomenclature indicates the type of RCA, with “P” for precast RCA and “T” for traditional RCA. For the third character of the nomenclature, the number “4” indicates that the aggregate replacement was based on target NA concrete mixture M-NA4, while the number “5” indicates replacement based on mixture M-NA5. The remaining two numbers on the specimen nomenclature indicate the replacement ratio  $R$ ,

expressed as a percentage (0, 50, or 100%), and the concrete age at superimposed loading,  $t_o$  (7 or 28 days), respectively.

The prestressing strands were passed through the wooden formwork and steel reinforcement cages, anchored on the dead-end bulkhead, and jacked and anchored to the specified force at the live end. The specified jacking force was ensured using a calibrated pressure gauge, and the final elongation of each strand was checked against the target elongation corresponding to the specified jacking force.

The beam specimens were cast in their as-tested configuration according to the daily procedures at Kerkstra Precast, Inc. For each mixture, approximately 1 yd<sup>3</sup> (0.76 m<sup>3</sup>) of concrete was batched to cast two identical (twin) 19 ft (5.79 m) long beams (one beam for each of 7- and 28-day superimposed loading), 3 x 6 in. (76 x 152 mm) concrete compressive strength and stiffness cylinders, and 6 x 6 x 21 in. (152 x 152 x 533 mm) modulus of rupture (MOR) beams. For the Series UP5 and CT4 beams, additional 4 x 8 in. (102 x 203 mm) concrete cylinders were also cast for creep and shrinkage testing.

Following typical batching procedures at Kerkstra Precast, Inc., each concrete constituent was weighed according to the mixture design. First, all the sand was placed in the mixer. Air entrainer was then injected into the sand and all coarse aggregates were discharged into the mixer. After mixing for approximately 10 seconds, the cement was discharged and the components were mixed for approximately 20 seconds. Then, a reading was taken with a moisture probe to determine the moisture in the batch. Based on this reading and the mixture design, the amount of additional water was determined by the concrete batching software, weighed, and discharged. After 15 seconds of additional mixing, all liquid admixtures were added to the batch. The concrete constitu-

**Table 4—Beam specimen details**

Series	Beam ID	$f_{pj}^*$ , ksi	RCA type	Mixture ID	$R,^\dagger$ %	$t_o,^\ddagger$ days	Camber, in.	Date loaded	Date unloaded	$\tau,^\S$ days
UP4	UP4-0-7	189	RCA-PC3	M-NA4	0	7	3/4	6/22/2016	2/27/2017	250
	UP4-50-7	189	RCA-PC3	M-RCA15	50	7	13/16	6/22/2016	2/27/2017	250
	UP4-100-7	189	RCA-PC3	M-RCA16	100	7	15/16	6/22/2016	2/27/2017	250
	UP4-0-28	189	RCA-PC3	M-NA4	0	28	13/16	7/13/2016	11/3/2016	113
	UP4-50-28	189	RCA-PC3	M-RCA15	50	28	7/8	7/13/2016	11/3/2016	113
	UP4-100-28	189	RCA-PC3	M-RCA16	100	28	1	7/13/2016	11/3/2016	113
UP5	UP5-0-7	189	RCA-PC3	M-NA5	0	7	1	7/27/2016	2/27/2017	215
	UP5-50-7	189	RCA-PC3	M-RCA17	50	7	1-1/8	7/27/2016	2/27/2017	215
	UP5-100-7	189	RCA-PC3	M-RCA18	100	7	1-1/16	7/27/2016	2/27/2017	215
	UP5-0-28	189	RCA-PC3	M-NA5	0	28	7/8	8/17/2016	11/3/2016	78
	UP5-50-28	189	RCA-PC3	M-RCA17	50	28	7/8	8/17/2016	11/3/2016	78
	UP5-100-28	189	RCA-PC3	M-RCA18	100	28	15/16	8/17/2016	11/3/2016	78
CT4	CT4-0-7	135	RCA-T	M-NA4	0	7	5/8	11/16/2016	2/27/2017	103
	CT4-50-7	135	RCA-T	M-RCA19	50	7	3/4	11/16/2016	2/27/2017	103
	CT4-100-7	135	RCA-T	M-RCA20	100	7	13/16	11/16/2016	2/27/2017	103
	CT4-0-28	135	RCA-T	M-NA4	0	28	9/16	12/7/2016	2/27/2017	82
	CT4-50-28	135	RCA-T	M-RCA19	50	28	5/8	12/7/2016	2/27/2017	82
	CT4-100-28	135	RCA-T	M-RCA20	100	28	3/4	12/7/2016	2/27/2017	82

\* $f_{pj}$  is strand jacking stress.

† $R$  is coarse aggregate replacement ratio (Eq. (1)).

‡ $t_o$  is concrete age at superimposed loading.

§ $\tau$  is superimposed loading duration.

Notes: 1 ksi = 6.89 MPa; 1 in. = 25.4 mm.

ents were then mixed for approximately 70 seconds and the batch was discharged.

Spread and air content measurements were immediately taken to qualify the concrete batch for use in the test specimens. Despite being within the target spread, Mixture M-RCA17 for the beams with  $R = 0.5$  appeared wetter than the corresponding  $R = 0$  and  $R = 1.0$  mixtures during the casting of the Series UP5 beams. Thus, the moisture and/or water measurement for  $R = 0.5$  may have been slightly off, possibly resulting in more water being included in the mixture, which would have effects on the concrete compressive strength and stiffness as well as creep and shrinkage.

Approximately 2 hours after casting, the beams and companion material specimens were covered with tarp (to reduce moisture and heat loss) and allowed to cure on the prestressing bed for approximately 18 hours. At this point, three compressive strength cylinders were tested to ensure appropriate concrete strength gain, after which the prestressing strands were cut simultaneously to transfer the prestress force into the concrete (that is, prestress transfer age of  $t_i = 18$  hours).

### Beam test setup

After prestress transfer, the beams were brought to the laboratory at the University of Notre Dame and subjected to a total superimposed service load of  $W_s = 4705$  lb (2134 kg) through four-point bending, as shown in Fig. 1, for at least 78 days. The clear span length between simple supports was

$l_s = 18$  ft (5.49 m), resulting in a clear span-depth aspect ratio of  $l_s/h = 24$ . The superimposed load was applied by placing a concrete weight block on two steel shims at  $\pm 12$  in. ( $\pm 305$  mm) on either side of the beam midspan. To apply the load with as little impact as possible, four screw jacks were used to initially support the block, which were slowly and uniformly lowered until the block was in contact with the steel shims.

A total of 12 concrete weight blocks were cast for simultaneous testing of 12 beams. Each block was sealed with two coats of masonry water-proofer and two coats of paint to maintain a consistent weight by minimizing moisture loss. Additionally, sealed buckets of sand were placed on each block to correct any small discrepancies in the block weights to achieve the target load of  $W_s = 4705$  lb (2134 kg).

This block weight was determined to induce a maximum immediate concrete compressive stress of approximately 50% of the allowable compressive stress  $\bar{\sigma}_{cs} = 0.45f'_{c,t_o}$  (based on ACI 318<sup>12</sup>) under prestress plus sustained load (that is, superimposed load plus beam self-weight) at the top of the uncracked (Class U) beams, where  $f'_{c,t_o}$  was the concrete compressive strength at the time  $t_o$  of superimposed load application. The corresponding maximum concrete tensile stress at the bottom of the beam section was approximately  $2.5\sqrt{f'_{c,t_o}}$ . In the cracked (Class C) beams, the applied loading induced a maximum immediate concrete stress of about 80% of  $\bar{\sigma}_{cs}$  in compression (at top) and about  $18\sqrt{f'_{c,t_o}}$  in tension (at bottom) calculated using the gross moment of

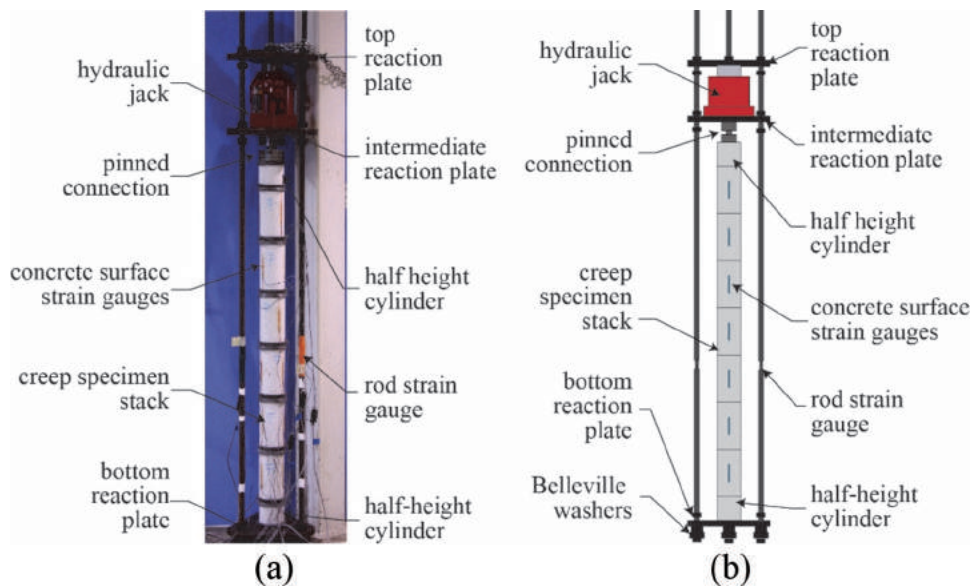


Fig. 3—Self-reacting creep frame: (a) photograph; and (b) schematic.

inertia, and a maximum immediate concrete stress of approximately 108% of  $\bar{\sigma}_{cs}$  in compression using the cracked transformed section moment of inertia ( $I'_{c,t_0}$  defined later in the paper).

In each series of tests, three beams (with  $R = 0, 0.5,$  and  $1$ ) were subjected to superimposed loading at a concrete age  $t_0$  of 7 days, and another set of three beams (again with  $R = 0, 0.5,$  and  $1$ ) were loaded at  $t_0$  of 28 days. Table 4 shows the details of the test variables, including the approximate midspan camber deflection (under prestress plus self-weight) prior to superimposed loading, superimposed loading/unloading dates, and the total superimposed loading duration  $\tau$ . The tests were not conducted in an environmental chamber; however, the beams with  $R = 0, 0.5,$  and  $1.0$  in each set were tested adjacent to each other and during the same time span, and, thus, any effects from changes in laboratory temperature and/or humidity were consistent between the three beams.

### Beam measurements

Prior to concrete casting, embedded vibrating wire strain gauges were placed at the depth  $d_p$  of the prestressing strands in one set ( $R = 0, 0.5,$  and  $1.0$ ) of beams to measure the concrete strains adjacent to the prestressing strands at the time of prestress transfer and afterward. In the Series UP4 beams, four gauges were placed at 1, 2, 3.5, and 5.5 ft (0.30, 0.61, 1.07, and 1.68 m) from the live (jacking) end of each beam. In the Series UP5 and CT4 beams, two more gauges were added at 0.5 and 1.5 ft (0.15 and 0.46 m) from the live end. Readings from the embedded gauges were taken immediately before and after prestress transfer. Additional readings were taken daily prior to superimposed loading, and then every hour for at least the first 3 hours after loading, at least daily for the first week of loading, at least weekly for the first month of loading, and at least biweekly for the remainder of service-load testing.

Midspan deflections of each beam were measured using a linear potentiometer and a data logger. The linear poten-

tiometer was attached at the centerline of the beam on the bottom surface. Measurements were taken every 20 seconds during the initial placement of superimposed loading and for approximately the first hour, and then every 15 minutes for the remainder of service-load testing.

### Companion creep and shrinkage cylinder measurements

Creep and shrinkage strain measurements were made on companion concrete cylinders for the Series UP4 and CT4 beams. The creep cylinders were capped using a sulfur compound to ensure that the cylinder ends were smooth and normal to the axis of the specimen for uniform loading in the creep frames. The shrinkage cylinders were also capped in the same way to achieve the same environmental boundary conditions as the creep cylinders. All cylinders were kept in the same facility and near the beam specimens, so any effects from temperature and humidity variations were consistent between the beam, creep, and shrinkage measurements. The creep tests for each series included cylinders loaded at  $t_0 = 7$  days as well as at 28 days.

Prior to initial creep loading, three cylinders for each  $R$  were tested to determine the compressive strength,  $f'_{c,t_0}$  of the concrete. Then, a total of six 4 x 8 in. (102 x 203 mm) cylinders (two for each of  $R = 0, 0.5,$  and  $1$ ) were stacked, and a load of approximately 40% of the lowest  $f'_{c,t_0}$  of the concrete in the stack was applied using a hydraulic jack and a self-reacting steel creep test frame as shown in Fig. 3 (similar to the creep loading procedure described in Knaack and Kurama<sup>2</sup>). The load on the creep cylinders was measured using strain gauges attached to the loading rods of the self-reacting frame. A range of  $\pm 5\%$  of the initial load was maintained by applying additional load using the jack as necessary throughout the creep testing duration.

The axial strains of the creep and shrinkage cylinders were measured using three concrete surface strain gauges equally spaced (that is, at 120-degree intervals) along the circumference of each cylinder at midheight. Applied load

**Table 5—Concrete material properties**

Beam ID	Spread, in.	$t = t_i = \sim 18$ hours		$t = t_o = 7$ days		$t = t_o = 28$ days		
		$f_{ci}^*$ , psi	$E_{ci}^*$ , psi	$f'_{c,t_o,\dagger}$ , psi	$E_{c,t_o,\dagger}$ , psi	$f'_{c,t_o,\ddagger}$ , psi	$E_{c,t_o,\ddagger}$ , psi	$f'_{t,t_o,\S}$ , psi
UP4-0-7/28	22.5	6077	4,747,140	8076	5,562,669	9559	5,768,663	768
UP4-50-7/28	21.0	6400	4,727,113	8764	5,412,045	9,855	5,564,224	845
UP4-100-7/28	21.5	6410	4,453,795	8578	4,939,320	10,167	5,123,049	754
UP5-0-7/28	21.5	5588	3,286,624	7294	4,234,450	8417	4,749,102	854
UP5-50-7/28	21.5	4959	3,101,669	7091	4,027,826	8424	4,892,538	759
UP5-100-7/28	20.5	5676	3,262,845	7797	4,005,215	9046	4,489,122	780
CT4-0-7/28	21.75	4489	4,241,704	7016	5,086,376	8748	5,383,054	563
CT4-50-7/28	23.75	4345	4,000,725	7014	4,642,350	8869	4,969,548	488
CT4-100-7/28	19.0	4129	3,739,579	7239	4,496,065	9008	4,875,110	506

\* $f_{ci}$  and  $E_{ci}$  are concrete compressive strength and stiffness at time of prestress transfer, respectively.

† $f'_{c,t_o}$  and  $E_{c,t_o}$  are concrete compressive strength and stiffness at time of superimposed loading (7 days or 28 days), respectively.

‡ $f'_{c,t_o}$  is concrete tensile strength (modulus of rupture) at 28 days.

Notes: 1 in. = 25.4 mm; 1 psi = 6895 Pa.

**Table 6—Prestressing strand properties**

Strand ID	Beam series	Measured				Certification sheet			
		$A_p^*$ , in.	$E_p^\dagger$ , ksi	$f_{pu}^\ddagger$ , ksi	$\epsilon_{pu}^\S$ , in./in.	$A_p^*$ , in.	$E_p^\dagger$ , ksi	$f_{pu}^\ddagger$ , ksi	$\epsilon_{pu}^\S$ , in./in.
S-0.5B2	UP4	0.150	30,759	293.4	0.0651	0.153	29,000	287.0	0.070
S-0.5B3	UP5	0.150	30,171	291.0	0.0751	0.153	29,000	286.6	0.072
S-0.5B4	CT4	0.149	30,219	289.3	0.0677	0.153	28,800	282.4	0.065

\* $A_p$  is cross-sectional area.

† $E_p$  is linear-elastic modulus.

‡ $f_{pu}$  is peak (ultimate) strength.

§ $\epsilon_{pu}$  is ultimate (fracture) strain.

Note: 1 in = 25.4 mm; 1 ksi = 6.89 MPa.

and concrete strain readings were taken every 20 seconds for an hour during and after the initial application of load using the hydraulic jack, and then every 15 minutes for the remainder of testing.

**Properties of concrete and prestressing steel strand**

The compressive strength  $f'_c$  and stiffness  $E_c$  of each concrete mixture were measured<sup>19</sup> by testing 3 x 6 in. (76 x 152.40 mm) cylinders at the prestress transfer age of  $t_i = 18$  hours (that is, initial  $f_{ci}'$  and  $E_{ci}$  at prestress transfer) as well as superimposed loading ages of  $t_o = 7$  and 28 days (with three cylinders tested at each age) according to ASTM C39<sup>20</sup> and C469.<sup>21</sup> The concrete tensile strength  $f'_t$  was measured from three MOR beams tested at 28 days under three-point bending with an 18 in. (457 mm) span length per ASTM C293.<sup>22</sup> Table 5 shows the measured average concrete properties for each mixture in each series, including spread, which was measured according to ASTM C1611.<sup>23</sup>

Differences in temperature and humidity inside the precast production plant at the time of casting may have caused variations in the strength of the summer-cast UP4-0 and winter-cast CT4-0 series specimens, which used the same concrete mixture design. In most cases, RCA led to an increase in the concrete compressive strength (but not necessarily on the tensile strength), which can be attributed to the high

quality and low deleterious material content of the RCA. Conversely, the use of RCA led to a reduction in the concrete stiffness in almost all cases. This was expected due to the presence of residual mortar in the RCA,<sup>1</sup> which was less stiff than the crushed limestone it replaced.

The prestressing strand was seven-wire, uncoated, low-relaxation steel that satisfied ASTM A416.<sup>24</sup> Three different strand spools from the same manufacturer were used for the three series. For each spool, the cross-sectional area  $A_p$  of the strand was determined using the measured weight of strand samples, as described in Walsh and Kurama.<sup>25</sup> Additionally, three strand samples were tested in tension, using special “sand-grip” anchors<sup>25,26</sup> to determine the strand stress versus strain behavior up to fracture. An extensometer with a 2 in. (51 mm) gauge length was used to measure the strand strains during each test. As allowed by ASTM A370,<sup>27</sup> the extensometer was removed at a stress of approximately 260 ksi (1793 MPa) (to prevent damage to the sensor from strand fracture), with the subsequent incremental (that is, additional) strand strains determined from the relative displacements of the testing machine crossheads. Table 6 shows the measured properties as well as properties from the manufacturer certification sheet for each of the three strand spools, including linear-elastic (Young’s) modulus  $E_p$ , peak (ultimate) strength at fracture  $f_{pu}$ , and ultimate strain at fracture  $\epsilon_{pu}$ .

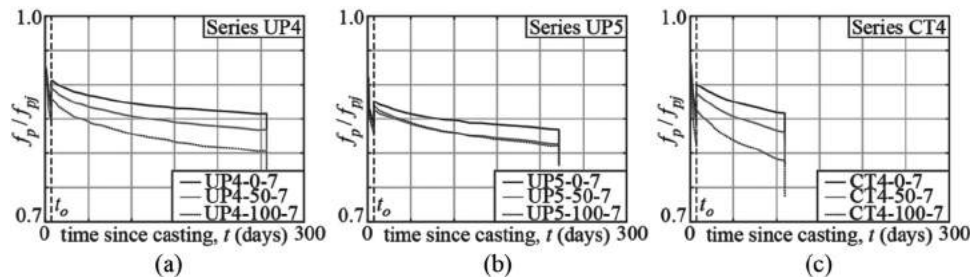


Fig. 4—Variation of strand stress over time: (a) UP4; (b) UP5; and (c) CT4.

## EXPERIMENTAL RESULTS

### Prestress losses

Prestress losses were measured using the embedded vibrating wire gauges. In this method, it was assumed that full prestress transfer was achieved at the location of the two gauges furthest away from the beam end (that is, located at 3.5 and 5.5 ft [1.07 and 1.68 m], where the strain measurements were similar) and that perfect bond existed between the concrete and steel strand. By averaging the readings from the two furthest gauges from the beam end, a drop in prestressing steel strain was determined immediately upon transfer, which was used to estimate the prestress loss  $\Delta f_p$ . The initial strand stress  $f_{pi}$  after transfer was calculated as the jacking stress  $f_{pj}$  minus  $\Delta f_p$ . The initial prestress losses increased by a very small amount (for example, by approximately 1% of the jacking stress for  $R = 1.0$ ) with the use of RCA.

This prestress loss calculation procedure was repeated using the measured strains (from the two furthest embedded vibrating wire gauges) throughout each test to determine the long-term prestress losses and remaining effective prestress immediately prior to superimposed load application,  $f_{p,t_0}$ , and after removal of superimposed load,  $f_{p,t_0+\tau}$ . The variation of strand stresses (normalized with respect to the jacking stress  $f_{pj}$ ) over time is given in Fig. 4. The long-term prestress losses increased with increasing  $R$  (for example, by 2 to 7% of the initial stress for  $R = 1.0$ ), which can be attributed to the greater creep and shrinkage strains of concrete with increased  $R$ .

### Cracking

As anticipated by design, beams from all three series experienced flexural cracking of the top upon prestress transfer, regardless of  $R$ . A lower number of cracks developed in the Series CT4 beams because of the reduced amount of prestress. The prestress-induced cracks occurred at a fairly uniform spacing over the beam top and were closed upon the subsequent application of superimposed load. Also, as designed, Series UP4 and UP5 (Class U) beams with  $f_{pj} = 0.7f_{pu}$  did not develop any flexural cracking at the bottom, while Series CT4 (Class C) beams with  $f_{pj} = 0.5f_{pu}$  cracked immediately upon the application of superimposed load. Figure 5 shows the observed superimposed load-induced cracking in the Series CT4 beams. Note that the cracks were hairline width, but were highlighted with a marker for ease of viewing. In general, the crack patterns and crack lengths appeared similar between the beams with  $R = 0, 0.5$ , and  $1.0$  loaded at  $t_0 = 7$  days. However, increases in the number and length of

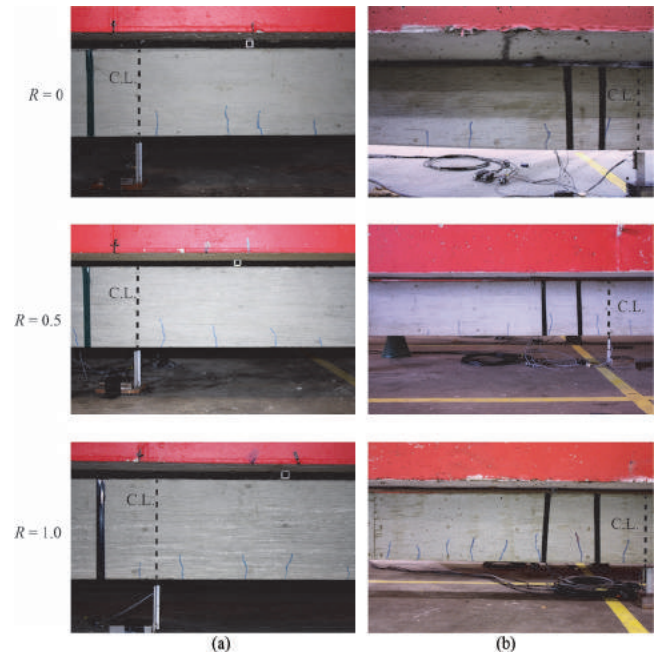


Fig. 5—Flexural cracking in CT4 series beams ( $R = 0$  [top row];  $R = 0.5$  [middle row]; and  $R = 1.0$  [bottom row]): (a)  $t_0 = 7$  days; and (b)  $t_0 = 28$  days.

cracking were observed between the beams with  $R = 0$  and  $1.0$  loaded at  $t_0 = 28$  days. These increases may have occurred because of the reduced tensile strength  $f'_t$  of RCA concrete as well as the increased prestresses losses  $\Delta f_p$ , as shown in Table 5 and Fig. 4, respectively.

### Shrinkage and creep strains

The measured shrinkage strains  $\epsilon_{sh,t'}$  from the unloaded concrete cylinders (average measurement from the three strain gauges on each cylinder) accompanying the Series UP5 and CT4 beams are shown in Fig. 6(a), where  $t' = t - t_0$  is the time since superimposed loading of the corresponding beam and creep specimens. Even though shrinkage strains started to accumulate from concrete casting at time  $t = 0$ , the measured shrinkage strains were initialized (that is, zeroed) at superimposed loading of the beam and creep specimens at time  $t = t_0$ . It can be seen that the incremental (that is, from time  $t = t_0$ ) shrinkage strains increased with  $R$ . The amplification of shrinkage strains (Fig. 6(b)) for  $R = 0.5$  and  $1.0$  (with respect to  $R = 0$ ) showed significant variation during the early stages (due to possible measurement errors of small strains), but stabilized during the later stages of the tests. These shrinkage amplifications were calculated by dividing

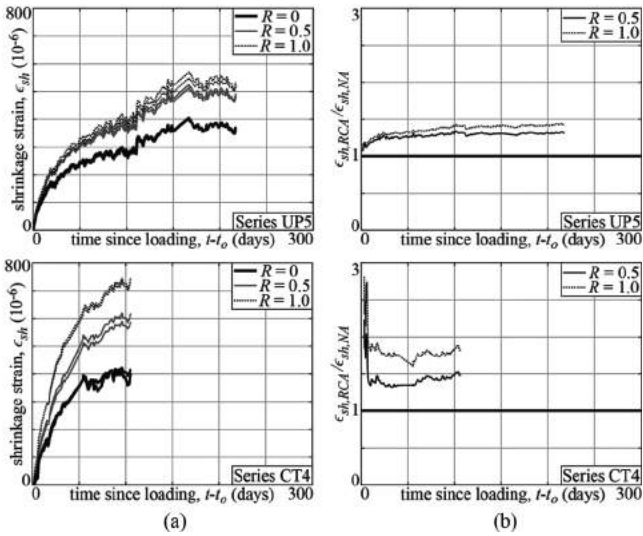


Fig. 6—Shrinkage cylinder results: (a) shrinkage strain; and (b) amplification.

the average total (that is, not incremental) shrinkage strain of the two RCA concrete cylinders (for each  $R$ ) by the average total shrinkage strain of the two corresponding NA concrete cylinders. In the Series UP5 specimens with precast RCA, the shrinkage strain amplifications for  $R = 0.5$  and  $1.0$  were approximately 1.30 and 1.40, respectively, at the end of testing. In comparison, the shrinkage strain amplifications for the Series CT4 specimens with traditional RCA were approximately 1.50 and 1.80 for  $R = 0.5$  and  $1.0$ , respectively. These results indicate that the concrete with traditional RCA (from construction demolition) underwent greater shrinkage strains than the concrete with precast RCA, which is likely related to the greater water absorption of the traditional RCA (Table 1).

Figure 7 shows the corresponding creep coefficient  $C_{c,t}$  for Series UP5 and CT4 specimens, calculated as

$$C_{c,t} = \varepsilon_{c,t} / \varepsilon_m \quad (2)$$

where  $\varepsilon_{c,t}$  is measured creep strain at superimposed loading duration  $t'$ , and  $\varepsilon_m$  is initial mechanical strain measured immediately after loading of the creep cylinders at time  $t = t_o$  (that is, at  $t' = 0$ ). The creep strain  $\varepsilon_{c,t}$  was found by subtracting the measured initial mechanical strain  $\varepsilon_m$  and incremental shrinkage strain  $\varepsilon_{sh,t}$  (that is, initialized at time  $t = t_o$ ) from the total measured creep cylinder strain (taken as the average measurement from the three strain gauges on each creep cylinder). The shrinkage strain to adjust the creep strain data was determined as the average of the six strain gauges on the two corresponding shrinkage cylinders.

Similar to the shrinkage strains, the creep coefficients were greater for RCA concrete and the creep coefficient amplifications remained relatively stable over time. Further, the creep coefficients were generally greater for the Series CT4 specimens than the Series UP5 specimens. However, unlike the shrinkage strain amplifications, the differences between the creep coefficient amplifications of the Series UP5 and Series CT4 specimens were not consistent. Additionally, no trend was observable for cylinders loaded at different

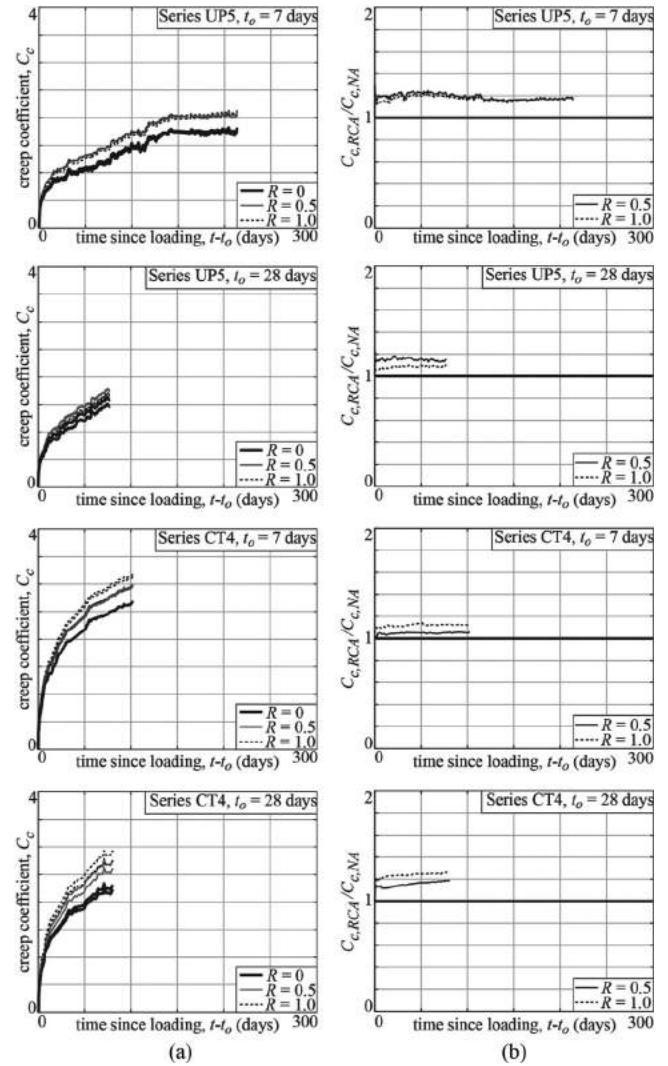


Fig. 7—Creep cylinder results: (a) creep coefficient; and (b) amplification.

ages (that is,  $t_o = 7$  or 28 days). These results may point to possible errors in the measurement of small strains (such as the initial mechanical strain  $\varepsilon_m$ ), resulting in errors in the calculation of the creep coefficient as discussed in Knaack and Kurama.<sup>2</sup> Also, as mentioned previously, the creep and shrinkage for the Series UP5 specimens with  $R = 0.5$  may have been affected by the possible use of excess water during the batching of this mixture (Mixture M-RCA17).

The measured creep coefficients were used to estimate the beam deflections described later in the paper. The creep coefficients  $C_{c,t_o}$  and  $C_{c,\tau}$  (at loading durations of  $t' = t_o$  and  $\tau$ , respectively) that were used specifically in these estimations are presented in Table 7, and were taken as averages of the measured values from each pair of creep cylinders. The concrete stiffnesses calculated from the measured initial mechanical strains  $\varepsilon_m$  of the creep cylinders are also listed. Note that the beam deflection estimations require the creep coefficient  $C_{c,t_o+\tau}$  at a loading duration of  $t' = t_o + \tau$  as well. Because the creep and shrinkage cylinder tests were only run for the duration of beam superimposed loading (that is, over a duration of  $t' = \tau$ ),  $C_{c,t_o+\tau}$  was estimated by extrapolating the creep data for  $C_{c,\tau}$  as

$$C_{c,t_0+\tau} = C_{c,t_0} [(t_0 + \tau)^{0.6} / [10 + \tau^{0.6}]] / \{\tau^{0.6} [10 + (t_0 + \tau)^{0.6}]\} \quad (3)$$

where the time-dependent form of Eq. (3) was taken from Branson and Kripanarayanan,<sup>28</sup> Branson,<sup>29</sup> and ACI 209R.<sup>30</sup> Note that other formulations, such as the method described in the *fib* Model Code for Concrete Structures,<sup>31</sup> can also be used to fit the creep coefficient.

### Midspan deflections

Figure 8 plots the measured midspan deflection  $\Delta$  of each beam versus time from the application of superimposed loading (measured deflections prior to superimposed loading are also shown for the Series UP5 and CT4 beams). Note that

**Table 7—Creep coefficients**

Beam ID	Measured			Extrapolated
	$E_{c,t_0}$ , * psi	$C_{c,t_0}$ †	$C_{c,\tau}$ †	$C_{c,t_0+\tau}$ †
UP5-0-7	5,194,830	0.66	1.78	1.79
UP5-50-7	4,286,420	0.76	2.08	2.09
UP5-100-7	4,172,480	0.76	2.09	2.11
UP5-0-28	5,394,120	1.06	1.56	1.68
UP5-50-28	4,339,390	1.13	1.78	1.91
UP5-100-28	3,624,470	1.15	1.70	1.83
CT4-0-7	4,639,460	1.21	2.82	2.86
CT4-50-7	4,242,070	1.27	2.98	3.02
CT4-100-7	4,128,150	1.33	3.16	3.20
CT4-0-28	4,875,340	1.65	2.27	2.44
CT4-50-28	4,695,360	1.89	2.70	2.89
CT4-100-28	4,262,490	2.04	2.86	3.06

\*Calculated from measured mechanical strains of creep cylinders.

†  $C_{c,t_0}$ ,  $C_{c,\tau}$ , and  $C_{c,t_0+\tau}$  are creep coefficients for loading durations of  $t' = t_0$ ,  $\tau$ , and  $t_0 + \tau$ , respectively.

Note: 1 psi = 6895 Pa.

all deflections were measured from the cambered position of each beam and were initialized (that is, zeroed) right before the application of superimposed loading. In most cases, an increase in  $R$  corresponded to an increase in deflections. The only exception can be seen in Fig. 8(b), where Beam UP5-50-7 deflected more than Beam UP5-100-7. Again, this may have been because of the possible addition of more water in the concrete mixture for Beam UP5-50-7 than for Beam UP5-100-7, as stated previously.

Deflection amplifications were determined by dividing the deflections of the RCA concrete beams by the deflections of the corresponding NA concrete beam in each set. From Fig. 9, it can be seen that the amplification of deflection did not vary much with time, as for the shrinkage and creep amplifications discussed previously. The largest deflection amplifications were in the cracked Beams CT4-100-7 and CT4-100-28 with full replacement ( $R = 1.0$ ) using traditional RCA, where the deflection at the end of testing was 1.25 and 1.37 times that of the corresponding NA concrete beam, respectively. The deflection amplifications decreased significantly with reduced amounts of RCA (for example, the amplification was 1.14 for Beam CT4-50-28 with  $R = 0.5$ ).

The deflection amplifications were much smaller for the uncracked Series UP4 and UP5 beams with precast RCA, ranging between 1.02 and 1.17 at full aggregate replacement ( $R = 1.0$ ). Overall, Fig. 9 shows that the use of precast RCA (Series UP4 and UP5 beams) resulted in smaller deflection amplifications than the traditional RCA (Series CT4 beams). This is consistent with the generally smaller shrinkage strain amplifications for concrete using precast RCA, as discussed previously (Fig. 6). It should be noted, however, that the differences between the creep coefficient amplifications of precast RCA and traditional RCA were mixed (Fig. 7), and as an additional difference, the beams with traditional RCA were designed to crack (Class C), whereas the beams with precast RCA were uncracked (Class U). Importantly, the deflection amplifications of the uncracked Series UP5

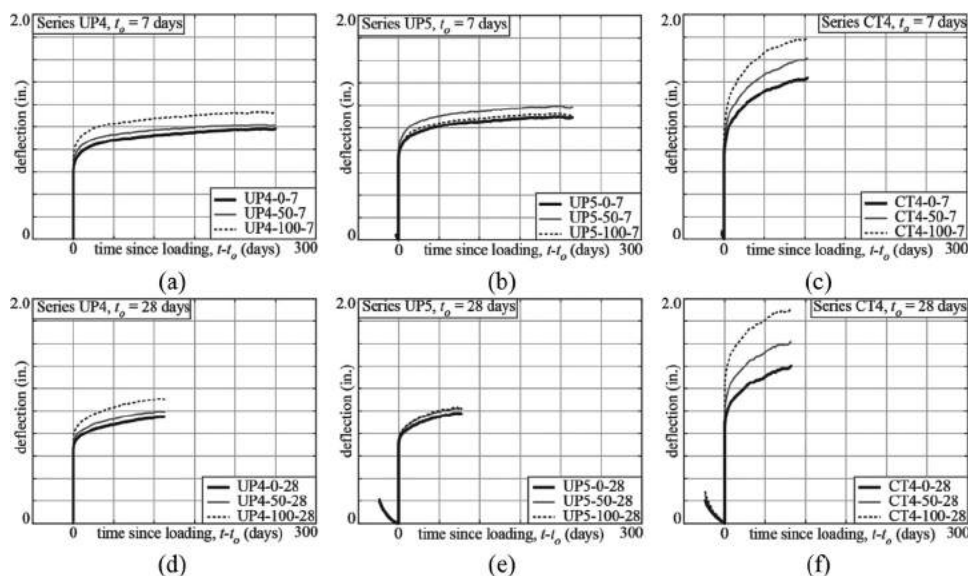


Fig. 8—Midspan deflection: (a) UP4,  $t_0 = 7$  days; (b) UP5,  $t_0 = 7$  days; (c) CT4,  $t_0 = 7$  days; (d) UP4,  $t_0 = 28$  days; (e) UP5,  $t_0 = 28$  days; and (f) CT4,  $t_0 = 28$  days. (Note: 1 in. = 25.4 mm.)

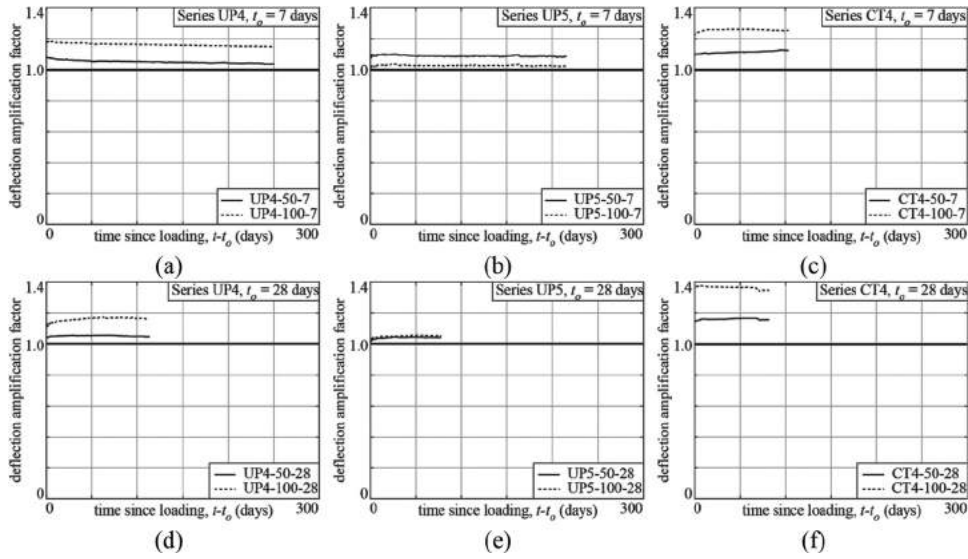


Fig. 9—Deflection amplification: (a) UP4,  $t_0 = 7$  days; (b) UP5,  $t_0 = 7$  days; (c) CT4,  $t_0 = 7$  days; (d) UP4,  $t_0 = 28$  days; (e) UP5,  $t_0 = 28$  days; and (f) CT4,  $t_0 = 28$  days.

beams with precast RCA were significantly smaller than the corresponding shrinkage and creep amplifications in Fig. 6 and 7, respectively. The deflection amplifications of the cracked Series CT4 beams with traditional RCA were also smaller than the shrinkage amplifications, but were similar to the creep amplifications. Some of the differences between the deflection, shrinkage, and creep amplifications may have been because of size differences between the specimens as well as differences in loading (for example, concrete in the beam specimens was subjected to varying compression and tension, while the creep cylinders were subjected to uniform compression).

### DESIGN ESTIMATIONS

The measured immediate and long-term midspan deflections,  $\Delta_{t_0}$  and  $\Delta_{t_0+\tau}$ , respectively, of the test specimens under superimposed loading were compared with closed-form design estimations (Table 8). Because the measured deflections were initialized (that is, zeroed) immediately before the superimposed loading at time  $t = t_0$ , the estimated deflections were also initialized at  $t = t_0$  by not including the deflections due to prestress and self-weight prior to  $t_0$ .

The immediate deflection  $\Delta_{t_0}$  due to superimposed loading was calculated as

$$\Delta_{t_0} = \Delta_{s,t_0} + \Delta'_{p,t_0} - \Delta_{p,t_0} + \Delta'_{g,t_0} - \Delta_{g,t_0} \quad (4)$$

where  $\Delta_{s,t_0}$  is initial deflection increment from the application of superimposed load;  $\Delta'_{p,t_0}$  and  $\Delta_{p,t_0}$  are deflections due to prestress force immediately after and immediately before the application of superimposed load, respectively; and  $\Delta'_{g,t_0}$  and  $\Delta_{g,t_0}$  are deflection due to beam self-weight immediately after and immediately before the application of superimposed load, respectively. These deflection components (positive downward) at time  $t = t_0$  were estimated using reinforced concrete beam theory as

$$\Delta_{s,t_0} = 0.5W_s a(3l_s^2 - 4a^2)/(24E_{c,t_0} I'_{e,t_0}) \quad (5)$$

$$\Delta_{p,t_0} = -P_{t_0} e l_s^2 / (8E_{c,t_0} I_{c,t_0}) \quad (6)$$

$$\Delta'_{p,t_0} = -P_{t_0} e l_s^2 / (8E_{c,t_0} I'_{e,t_0}) \quad (7)$$

$$\Delta_{g,t_0} = 5w l_s^4 / (384E_{c,t_0} I_{c,t_0}) \quad (8)$$

$$\Delta'_{g,t_0} = 5w l_s^4 / (384E_{c,t_0} I'_{e,t_0}) \quad (9)$$

where  $W_s$  is total superimposed load (4705 lb [2134 kg]);  $a$  is distance from simple support to point of superimposed load (8 ft [2.44 m]);  $l_s$  is clear span length (18 ft [5.49 m]);  $E_{c,t_0}$  is concrete stiffness at  $t = t_0$  (refer to Table 5);  $P_{t_0}$  is prestress force right before the application of superimposed load at  $t = t_0$  (using the measured strand stresses from Fig. 4);  $e$  is prestress eccentricity (3 in. [76.2 mm]);  $w$  is distributed self-weight of the beam (56.3 lb/ft [83.7 kg/m]);  $I_{c,t_0}$  is cracked transformed section moment of inertia of beam immediately prior to the application of superimposed load; and  $I'_{e,t_0}$  is effective moment of inertia of beam immediately after the application of superimposed load.

Upon prestress transfer, both the Class U and Class C beams were designed to experience cracking at the top, which was observed over the entire span length of the specimens. The effect of this cracking on  $\Delta_{p,t_0}$  and  $\Delta_{g,t_0}$  was quantified in Eq. (6) and (8) by using  $I_{c,t_0}$ , which was determined through cracked section analysis under prestress and self-weight together with measured values for  $E_{c,t_0}$  and  $P_{t_0}$ .

The application of the superimposed load,  $W_s$  caused the top cracks to close. The subsequent moment of inertia,  $I'_{e,t_0}$  was estimated as

$$\text{Class U beams: } I'_{e,t_0} = I_{u,t_0} \quad (10)$$

Class C beams:

$$I'_{e,t_0} = I_{u,t_0} (M_{c,t_0} / M_a)^3 + I_{c,t_0} [1 - (M_{c,t_0} / M_a)^3] \leq I_{u,t_0} \quad (11)$$

**Table 8—Measured and estimated immediate and long-term beam deflections**

Beam ID	$\tau$ ,* days	$\Delta_{t_0}^\dagger$			$\Delta_{t_0+\tau}^\ddagger$		
		Measured, in.	Estimated, in.	Estimated/measured	Measured, in.	Estimated, in.	Estimated/measured
UP4-0-7	250	0.55	0.76	1.38	0.98	—	—
UP4-50-7	250	0.61	0.73	1.21	1.02	—	—
UP4-100-7	250	0.66	0.81	1.23	1.13	—	—
UP4-0-28	113	0.62	0.74	1.19	0.95	—	—
UP4-50-28	113	0.64	0.71	1.12	1.00	—	—
UP4-100-28	113	0.68	0.78	1.14	1.11	—	—
UP5-0-7	215	0.67	0.85	1.28	1.10	1.54	1.41
UP5-50-7	215	0.70	0.84	1.20	1.19	1.69	1.43
UP5-100-7	215	0.66	0.85	1.29	1.12	1.71	1.52
UP5-0-28	78	0.68	0.77	1.15	0.98	1.56	1.59
UP5-50-28	78	0.68	0.73	1.07	1.03	1.54	1.50
UP5-100-28	78	0.68	0.77	1.14	1.04	1.65	1.59
CT4-0-7	103	0.67	0.72	1.07	1.44	2.00	1.39
CT4-50-7	103	0.73	0.81	1.10	1.62	2.37	1.47
CT4-100-7	103	0.82	0.83	1.01	1.80	2.59	1.44
CT4-0-28	82	0.80	0.69	0.86	1.40	1.88	1.34
CT4-50-28	82	0.91	0.78	0.85	1.62	2.36	1.45
CT4-100-28	82	1.07	0.79	0.73	1.92	2.54	1.33
			Average	1.11		Average	1.45
			Standard deviation	0.16		Standard deviation	0.09

\* $\tau$  is superimposed loading duration.

† $\Delta_{t_0}$  is immediate midspan deflection due to superimposed loading.

‡ $\Delta_{t_0+\tau}$  is total long-term midspan deflection at end of superimposed loading duration.

Note: 1 in. = 25.4 mm.

where  $I_{u,t_0}$  is moment of inertia of the uncracked transformed section (using  $E_{c,t_0}$ );  $I'_{c,t_0}$  is cracked transformed section moment of inertia immediately after the application of superimposed load (calculated using the measured strand stresses and corresponding force  $P'_o$  immediately after the application of superimposed load);  $M_{c,t_0}$  is cracking moment of the section (using  $E_{c,t_0}$  and  $P_o$  right before the application of superimposed load); and  $M_a$  is maximum moment along beam span due to superimposed load and self-weight. Equation (11) for the Class C beams was adapted from the well-known effective moment of inertia equation in ACI 318.<sup>12</sup>

The total long-term deflection at the end of the sustained loading period,  $\Delta_{t_0+\tau}$ , was determined as the sum of the initial deflection and the additional time-dependent deflection due to sustained loading as

$$\Delta_{t_0+\tau} = \Delta_{t_0} + (\alpha_{t_0+\tau} - \alpha_{t_0})\Delta_{pi} + (\beta_{t_0+\tau} - \beta_{t_0})\Delta_{gi} + \gamma_\tau \Delta_{s,t_0} \quad (12)$$

where  $\Delta_{t_0}$  and  $\Delta_{s,t_0}$  were determined from Eq. (4) and (5), respectively. The initial deflections due to prestress and self-weight,  $\Delta_{pi}$  and  $\Delta_{gi}$ , were determined using Eq. (6) and (8), respectively, but with  $E_{ci}$ ,  $P_i$ , and  $I_{ci}$  calculated at the time of prestress transfer (Table 5 and Fig. 4).

The time-dependent long-term multipliers,  $\alpha$ ,  $\beta$ , and  $\gamma$ , for the deflections due to prestress, self-weight, and superim-

posed load, respectively, were determined using the Branson Multiplier method<sup>28,29,32</sup> as

$$\alpha_{t_0} = (P_{t_0}/P_i) - 1 + 0.5(1 + P_{t_0}/P_i)C_{c,t_0} \quad (13)$$

$$\alpha_{t_0+\tau} = (P_{t_0+\tau}/P_i) - 1 + 0.5(1 + P_{t_0+\tau}/P_i)k_r C_{c,t_0+\tau} \quad (14)$$

$$\beta_{t_0} = C_{c,t_0} \quad (15)$$

$$\beta_{t_0+\tau} = k_r C_{c,t_0+\tau} \quad (16)$$

$$\gamma_\tau = k_r C_{c,\tau} \quad (17)$$

where  $P_{t_0+\tau}$  is force in the prestressing strands right after the removal of superimposed load at time  $t = t_0 + \tau$  (using measured stresses from Fig. 4); and  $C_{c,t_0}$ ,  $C_{c,\tau}$ , and  $C_{c,t_0+\tau}$  are creep coefficients for loading durations of  $t' = t_0$ ,  $\tau$ , and  $t_0 + \tau$ , respectively (refer to Table 7). Because no creep cylinders were tested for the Series UP4 beams, no estimation for  $\Delta_{t_0+\tau}$  was made for these specimens.

The coefficient  $k_r$  in Eq. (14), (16), and (17) represents the effect of the two U.S. No. 3 (No. M10) top bars used in the test specimens, based on the equation given in ACI 318<sup>12</sup> for compression reinforcement as

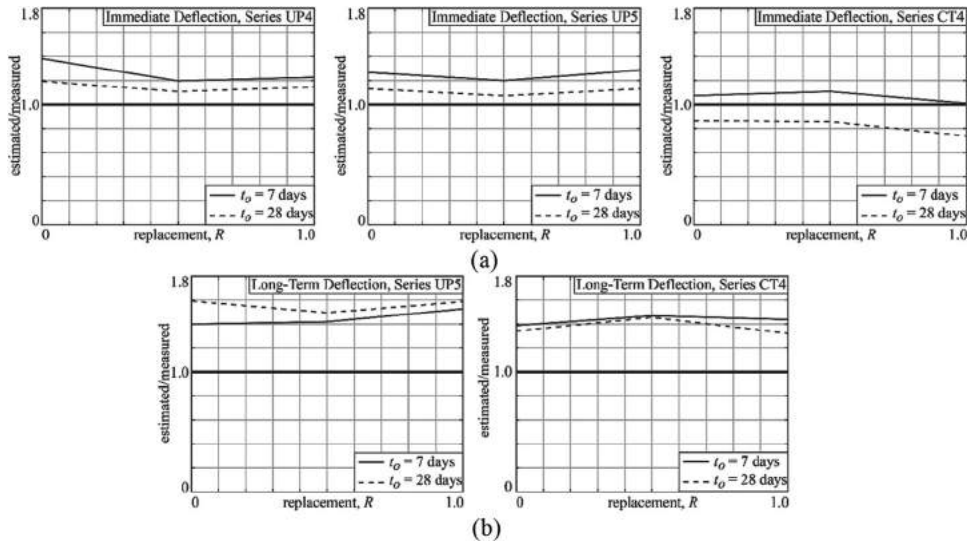


Fig. 10—Estimated versus measured beam midspan deflections: (a) immediate; and (b) long term.

$$k_r = 1/[1 + 50A_s'/(bd_p)] \quad (18)$$

where  $A_s'$  is total area of the compression bars (two U.S. No. 3 bars);  $b$  is beam width; and  $d_p$  is depth to prestressing strands from top of beam. Note that the  $k_r$  factor given by Eq. (18) is different from that given by Branson and Kripanarayanan.<sup>28</sup> This is because the  $k_r$  factor in Branson and Kripanarayanan represents the effect of non-prestressed tension reinforcement near the prestressing steel. Because none of the tested beams had non-prestressed steel near the strands, the  $k_r$  equation given by Branson and Kripanarayanan<sup>28</sup> was not used. Note also that no correction factor for age, humidity, specimen shape, or specimen size was used in the estimation of  $\Delta_{t_o+\tau}$ .

In the aforementioned procedure, the effect of RCA in the estimated deflections was accounted for by the generally decreased modulus of elasticity  $E_c$ , increased creep coefficient  $C_c$ , and increased prestress loss  $\Delta f_p$ , with increasing  $R$ . Comparisons of the measured deflections with the design estimations are shown in Table 8 and Fig. 10. The immediate deflections were over-estimated except for the Series CT4 beams loaded at  $t_o = 28$  days. For the long-term deflections, the Branson Multiplier Method over-estimated the measured deflections by an average of 45%. Because this method is dependent on the estimation of immediate deflections, it was affected by the immediate deflections that were overestimated for most of the beams. Importantly, the accuracy of the estimations for both immediate and long-term beam deflections was consistent regardless of the use of RCA. A fiber-based (that is, layered) numerical model was developed to estimate the long-term service-load deflections of non-prestressed RCA concrete beams<sup>33</sup>; however, this model has not yet been applied to prestressed RCA concrete beams.

## CONCLUSIONS

This paper experimentally investigated the use of RCA as a replacement for coarse natural aggregates in precast/prestressed concrete structures. The important conclusions are summarized as follows. Note that these results may be limited to the materials used and tests conducted.

1. Long-term prestress losses generally increased with increasing aggregate replacement ratio  $R$  (by approximately 2% to 7% for the beams with  $R = 1.0$  in this study), which can be attributed to the greater creep and shrinkage deformations of RCA concrete. The effect of RCA on short-term prestress losses was very small.

2. Superimposed load-induced crack patterns in Series CT4 were similar between the beams with  $R = 0, 0.5$ , and  $1.0$  loaded at  $t_o = 7$  days. Increases in the number and length of cracks occurred between the Series CT4 beams with  $R = 0$  and  $1.0$  loaded at  $t_o = 28$  days.

3. Concrete with traditional RCA (from construction demolition) underwent greater shrinkage strains than concrete with precast RCA, which is likely related to the greater water absorption of the traditional RCA used in this research. These results indicate that the quality of the precast RCA used in this research was superior to the quality of the construction demolition RCA.

4. Increased levels of RCA (that is, increased  $R$ ) led to increased immediate and long-term deflections of the beam test specimens under sustained service loads. An appropriate level of  $R$  must be considered when designing for deflection control.

5. The amplification of beam deflections due to the use of RCA did not vary much with time, as for the amplification of concrete creep and shrinkage with time. The largest deflection amplifications were measured in the cracked Beams CT4-100-7 and CT4-100-28 with full replacement ( $R = 1.0$ ) using traditional RCA, where the deflection at the end of testing was 1.25 and 1.37 times the deflection of the corresponding NA concrete beam, respectively. The deflection amplifications decreased significantly with reduced amounts of RCA (for example, the amplification was 1.14 for Beam CT4-50-28 with  $R = 0.5$ ).

6. The deflection amplifications were much smaller for the uncracked Series UP4 and UP5 beams with precast RCA, ranging between 1.02 and 1.17 at full aggregate replacement ( $R = 1.0$ ). Overall, the use of precast RCA (Series UP4 and UP5 beams) resulted in smaller deflection amplifications than traditional RCA (Series CT4 beams), which was

consistent with the smaller shrinkage strain amplifications for concrete using precast RCA.

7. The deflection amplifications of the uncracked Series UP5 beams with precast RCA were significantly smaller than the corresponding concrete shrinkage and creep strain amplifications. The deflection amplifications of the cracked Series CT4 beams with traditional RCA were also smaller than the shrinkage amplifications, but were similar to the creep amplifications.

8. Regardless of the amount of RCA, the immediate deflections of the beams were conservatively and consistently (that is, similarly for the beams with different  $R$ ) overestimated by current design code methods, except for the Series CT4 beams loaded at  $t_o = 28$  days, which were consistently underestimated by up to 27%. Similarly, the Branson Multiplier Method generally overestimated the measured long-term deflections of the beams regardless of  $R$ . These results imply that the ability of the design methods to predict the immediate and long-term deflections of the beams was not significantly affected by  $R$ .

### AUTHOR BIOS

**Michael R. Brandes** is a Design Engineer at Schaefer Inc., Cincinnati, OH. He received his MS and BS in civil engineering from the University of Notre Dame, Notre Dame, IN. His research interests include novel reinforced concrete design and sustainable concrete construction practices.

ACI member **Yahya Kurama** is a Professor in the Department of Civil and Environmental Engineering and Earth Sciences at the University of Notre Dame. He is a member of ACI Committees 374, Performance-Based Seismic Design of Concrete Structures; 555, Concrete with Recycled Materials; and Joint ACI-ASCE Committee 550, Precast Concrete Structures. His research interests include the behavior and design of reinforced concrete structures under extreme loading from earthquake and fire, sustainable construction, and precast/prestressed concrete structures.

### ACKNOWLEDGMENTS

This research is funded by the U.S. National Science Foundation (NSF) under Grant No. CMMI 1436758. The support of the current NSF Program Director Y. G. Hsuan and former NSF Program Director K. I. Mehta is gratefully acknowledged. The authors sincerely thank Kerkstra Precast, Inc., Grandville, MI, and West Michigan Recycle, Grandville, MI, for providing the RCA materials in this research. The beam casting was also conducted at Kerkstra Precast, Inc., which is gratefully acknowledged. Any opinions, findings, conclusions, and/or recommendations in the paper are those of the authors and do not necessarily represent the views of the NSF, the program directors, or other organizations acknowledged herein.

### REFERENCES

1. Knaack, A., and Kurama, Y., "Design of Normal Strength Concrete Mixtures with Recycled Concrete Aggregates," *ACI Materials Journal*, V. 110, No. 5, Sept.-Oct. 2013, pp. 483-493.
2. Knaack, A., and Kurama, Y., "Creep and Shrinkage of Normal Strength Concrete with Recycled Concrete Aggregates," *ACI Materials Journal*, V. 112, No. 3, May-June 2015, pp. 451-462. doi: 10.14359/51687392
3. Dhir, R.; Limbachiya, M.; and Leelawat, T., "Suitability of Recycled Concrete Aggregate for use in BS 5328 Designated Mixes," *Proceedings of the Institution of Civil Engineers. Structures and Buildings*, V. 134, No. 3, 1999, pp. 257-274. doi: 10.1680/istbu.1999.31568
4. Topçu, İ. B., and Şengel, S., "Properties of Concretes Produced with Waste Concrete Aggregate," *Cement and Concrete Research*, V. 34, No. 8, 2004, pp. 1307-1312. doi: 10.1016/j.cemconres.2003.12.019
5. Yamato, T., "Mechanical Properties, Drying Shrinkage and Resistance to Freezing and Thawing of Concrete using Recycled Aggregate," *Fourth CANMET/ACI/JCI Conference: Advances in Concrete Technology*, SP-179, American Concrete Institute, Farmington Hills, MI, 1998, pp. 105-121.
6. Fathifazl, G.; Razaqpur, A.; Isgor, O.; Abbas, A.; Fournier, B.; and Foo, S., "Creep and Drying Shrinkage Characteristics of Concrete Produced with Coarse Recycled Concrete Aggregate," *Cement and Concrete Composites*, V. 33, No. 10, 2011, pp. 1026-1037. doi: 10.1016/j.cemconcomp.2011.08.004

7. Knaack, A., and Kurama, Y., "Sustained Service-Load Behavior of Concrete Beams with Recycled Concrete Aggregates," *ACI Structural Journal*, V. 112, No. 5, Sept.-Oct. 2015, pp. 565-577. doi: 10.14359/51687799
8. Choi, W., and Yun, H., "Long-Term Deformations and Flexural Behavior of Reinforced-Concrete Beams with Recycled Aggregates," *Materials & Design*, V. 51, 2013, pp. 742-750. doi: 10.1016/j.matdes.2013.04.044
9. Lapko, A., and Grygo, R., "Long Term Deflection of Recycled Aggregate Concrete (RAC) Beams Made of Recycled Concrete," *10th International Conference: Modern Building Materials, Structures and Techniques*. Vilnius, Lithuania, 2010, pp. 709-712.
10. Limbachiya, M.; Leelawat, T.; and Dhir, R., "Use of Recycled Concrete Aggregate in High-Strength Concrete," *Materials and Structures*, V. 33, No. 9, 2000, pp. 574-580. doi: 10.1007/BF02480538
11. Perez-Benedicto, J.; del Rio-Merino, M.; Peralta-Canudo, J.; and de la Rosa-La Mata, M., "Mechanical Characteristics of Concrete with Recycled Aggregates Coming from Prefabricated Discarded Units," *Materiales de Construcción*, V. 62, No. 305, 2012, pp. 25-37.
12. ACI Committee 318, "Building Code Requirements for Structural Concrete (ACI 318-14) and Commentary (ACI 318R-14)," American Concrete Institute, Farmington Hills, MI, 2014, 520 pp.
13. MDOT, "Standard Specifications for Construction," Michigan Department of Transportation, Lansing, MI, 2012, 1001 pp.
14. ASTM C127, "Standard Test Method for Relative Density (Specific Gravity) and Absorption of Coarse Aggregate," ASTM International, West Conshohocken, PA, 2015, 5 pp.
15. ASTM C128, "Standard Test Method for Relative Density (Specific Gravity) and Absorption of Fine Aggregate," ASTM International, West Conshohocken, PA, 2015, 6 pp.
16. ASTM C494, "Standard Specification for Chemical Admixtures for Concrete," ASTM International, West Conshohocken, PA, 2017, 10 pp.
17. ASTM C260, "Standard Specification for Air-Entraining Admixtures for Concrete," ASTM International, West Conshohocken, PA, 2016, 4 pp.
18. ASTM C150, "Standard Specification for Portland Cement," ASTM International, West Conshohocken, PA, 2017, 9 pp.
19. Brandes, M., and Kurama, Y., "Effect of Recycled Concrete Aggregates on Strength and Stiffness Gain of Concrete and on Bond Strength of Steel Prestressing Strand," *PCI Journal*, V. 63, No. 2, Mar.-Apr. 2018, pp. 87-105.
20. ASTM C39, "Standard Test Method for Compressive Strength of Cylindrical Concrete Specimens," ASTM International, West Conshohocken, PA, 2018, 8 pp.
21. ASTM C469, "Standard Test Method for Static Modulus of Elasticity and Poisson's Ratio of Concrete in Compression," ASTM International, West Conshohocken, PA, 2014, 5 pp.
22. ASTM C293, "Standard Test Method for Flexural Strength of Concrete (Using Simple Beam With Center-Point Loading)," ASTM International, West Conshohocken, PA, 2016, 4 pp.
23. ASTM C1611, "Standard Test Method for Slump Flow of Self-Consolidating Concrete," ASTM International, West Conshohocken, PA, 2014, 6 pp.
24. ASTM A416, "Standard Specification for Low-Relaxation, Seven-Wire Steel Strand for Prestressed Concrete," ASTM International, West Conshohocken, PA, 2017, 5 pp.
25. Walsh, K., and Kurama, Y., "Behavior of Unbonded Post-Tensioning Monostrand Anchorage Systems Under Monotonic Tensile Loading," *PCI Journal*, V. 55, No. 1, 2010, pp. 97-117. doi: 10.15554/pcij.01012010.97.117
26. Walsh, K., and Kurama, Y., "Effects of Loading Conditions on the Behavior of Unbonded Post-Tensioning Strand-Anchorage Systems," *PCI Journal*, V. 57, No. 1, 2012, pp. 76-96. doi: 10.15554/pcij.01012012.76.96
27. ASTM A370, "Standard Test Methods and Definitions for Mechanical Testing of Steel Products," ASTM International, West Conshohocken, PA, 2017, 50 pp.
28. Branson, D. E., and Kripanarayanan, K. M., "Loss of Prestress, Camber, and Deflections of Non-Composite and Composite Prestressed Concrete Structures," *PCI Journal*, V. 16, No. 5, 1971, pp. 22-52. doi: 10.15554/pcij.09011971.22.52
29. Branson, D., *Deformation of Concrete Structures*. McGraw-Hill, New York, 1977, 546 pp.
30. ACI Committee 209, "Prediction of Creep, Shrinkage, and Temperature Effects in Concrete Structures (ACI 209R-92)," American Concrete Institute, Farmington Hills, MI, 1992, 47 pp.
31. *fib*, "Model Code for Concrete Structures," International Federation for Structural Concrete, Lausanne, Switzerland, 2010, 436 pp.
32. Naaman, A., *Prestressed Concrete Analysis and Design: Fundamentals: 2nd Edition*, McGraw-Hill, New York, 2004, 1072 pp.
33. Knaack A., and Kurama, Y., "Modeling Time-Dependent Deformations: Application for Reinforced Concrete Beams with Recycled Concrete Aggregates," *ACI Structural Journal*, V. 115, No. 1, Jan. 2018, pp. 175-190.

**NOTES:**

---